

Invited Papers

Precise control of the global rotation of strongly coupled ion plasmas in a Penning trap*

X.-P. Huang,[†] J. J. Bollinger, T. B. Mitchell, and W. M. Itano

Time & Frequency Division, National Institute of Standards and Technology, Boulder, Colorado 80303

D. H. E. Dubin

Department of Physics, University of California at San Diego, La Jolla, California 92093

(Received 13 November 1997; accepted 5 January 1998)

Rotating asymmetric electric fields have been applied to control the rotation frequency (and hence the density) of non-neutral plasmas, which are confined in Penning-type traps and have relaxed close to thermal equilibrium characterized by a global rigid-body rotation. ‘‘Infinite’’ confinement times and density compression were first reported for uncorrelated plasmas of $\sim 10^8$ Mg^+ ions with temperatures ranging from 1 K to 5×10^4 K (4 eV) [Huang *et al.*, *Phys. Rev. Lett.* **78**, 875 (1997)]. In this paper, the rotating field technique has been applied to control strongly coupled plasmas of $\sim 10^5$ $^9\text{Be}^+$ ions which are laser-cooled to millikelvin temperatures so that the plasma freezes into a solid with a crystalline lattice. Here, Bragg diffraction peaks from crystals provide an accurate way of measuring the rotation frequency, and it is observed that the plasma rotation can be phase locked to the applied rotating field without any slip. In essence, these corotating plasmas have reached thermal equilibrium with the rotating field, and the azimuthally asymmetric boundaries of the equilibrium states have been measured experimentally. Both rotating dipole and quadrupole fields have been used to provide this precise control of the plasma rotation. However, the effectiveness of the dipole field depends on the presence of multiple ion species. With the rotating dipole field, density compression to near the Brillouin limit and increase of the rotation frequency to near the cyclotron frequency have been achieved. [S1070-664X(98)91105-3]

I. INTRODUCTION

Unneutralized plasmas with a single sign of charge are often confined in Penning-type traps^{1,2} for a variety of experiments including plasma physics,³ Coulomb crystal studies,^{4,5} precision spectroscopy,^{6,7} antimatter research,^{8,9} and storage of highly charged ions.¹⁰ Since there is an average radial electric field, these trapped non-neutral plasmas undergo a global ($\mathbf{E} \times \mathbf{B}$) rotation about the magnetic field axis. In principle, perfect confinement can be obtained in an ideal trap with cylindrical symmetry due to conservation of (canonical) angular momentum.¹¹ In practice, background neutral molecules¹²⁻¹⁴ and static field asymmetries^{12,15-18} exert an ambient drag on the rotating plasma, causing slow expansion and eventual particle loss. Radiation pressure from laser beams has been used to balance the angular momentum loss and to vary the plasma rotation frequency.^{19,20} However, this method is limited to the few ion species whose atomic transitions are accessible by a laser, and is not precise due to laser power, frequency, and pointing fluctuations. Recently, azimuthally asymmetric (‘‘rotating wall’’) electric fields rotating in the same sense as the plasma have been used to exert a torque on Mg^+ plasmas with temperatures

ranging from 1 K to 5×10^4 K (4 eV), resulting in steady-state confinement and density compression.²¹⁻²³ For these uncorrelated plasmas, the stabilized rotation frequency is somewhat less than that of the rotating field, with a slip frequency which increases with the plasma temperature.²²

In this paper we show that rotating wall electric fields applied to a Penning trap with quadratic potentials can control the rotation of laser-cooled, crystallized $^9\text{Be}^+$ plasmas without slip, thus extending the applicability of this technique from uncorrelated plasmas to strongly coupled systems.²⁴ Precise control of the plasma rotation is important for some applications. As an example, the second-order Doppler (time dilation) shift due to rotational velocity in a Penning trap atomic clock can be minimized by stabilizing the rotation at a particular frequency.⁷ Both axially independent dipole and quadrupole fields in the plane perpendicular to the magnetic field have been used to provide this precise control of the plasma rotation. However, experimental evidence suggests that the effectiveness of the dipole field requires the presence of more than one ion species or other nonideal effects.

The rotating field control, which relies on ion-ion interactions, is fundamentally different from the sideband cooling or ‘‘axialization’’ techniques, where rf fields convert single-

*Paper gTuaI2-2 Bull. Am. Phys. Soc. **42**, 1876 (1997).

[†]Invited speaker.

particle magnetron motion into damped axial or cyclotron motions.^{25–27} The steady-state sideband-cooled radius of the magnetron motion depends on the strength of the rf field and the damping rate of the motion to which the magnetron motion is being coupled. In general, the rotation control will be of limited precision and may be effective only for low rotation frequencies where the space-charge field is weak.²⁸ In contrast, the rotating fields interact with ions near the plasma surface, creating a small-amplitude traveling wave. The torque due to this wave is then transferred to the plasma interior through “viscosity” or strong ion-ion Coulomb coupling, which acts to bring the plasma to the same rotation frequency as the applied field.²⁹

In the present experiment, side-view images show that the plasma shape, which is determined by the rotation frequency, can be varied by slowly changing the rotating field frequency for both weakly and strongly coupled plasmas. When the plasma is sufficiently cold and crystalline lattices are formed, Bragg diffraction provides a more accurate measurement of the rotation frequency. It is observed that the lattice and its orientation can be stable for longer than 30 min ($\sim 10^8$ rotations), and its rotation can be phase locked to the rotating field during this time. In essence, these corotating plasmas have reached a novel global thermal equilibrium,²⁹ where the rotation frequency (and hence the density) is set precisely by the external drive. For the rotating quadrupole field we have measured the triaxial ellipsoidal surface of this equilibrium state for oblate (pancake-like) plasmas, and found quantitative agreement with the analytical theory. For the rotating dipole field applied to plasmas with contaminant ions we have observed the expected asymmetric distribution of the $^9\text{Be}^+$ ions in close agreement with Monte Carlo simulations. Control of the global rotation has been achieved for nearly all allowed rotation frequencies with the use of the rotating dipole field.

II. EXPERIMENTAL SETUP

Figure 1 shows the apparatus with its optical diagnostics and schematics of the rotating dipole and quadrupole fields. The trap consists of a 127 mm long stack of cylindrical electrodes at room temperature with an inner diameter of 40.6 mm, enclosed in a 10^{-8} Pa vacuum chamber. The uniform magnetic field $B_0 = 4.46$ T is aligned parallel to the trap axis within 0.01° , giving a $^9\text{Be}^+$ (charge e and mass m) cyclotron frequency $\Omega = eB_0/m = 2\pi \times 7.61$ MHz. An axisymmetric trapping potential $(m\omega_z^2/2e)[z^2 - (x^2 + y^2)/2]$ is generated near the trap center by biasing the central electrodes to a negative voltage $-V_0$. At $V_0 = 1$ kV, the single-particle axial frequency ω_z is $2\pi \times 799$ kHz and the magnetron frequency $\omega_m = (\Omega - \sqrt{\Omega^2 - 2\omega_z^2})/2$ is $2\pi \times 42.2$ kHz. The z -independent rotating fields are generated by applying properly phased sinusoidal voltages of amplitude V_w to the six-fold azimuthal sectors of the two compensation electrodes, which are positioned symmetrically in the axial direction with respect to the trap center.

We create $^9\text{Be}^+$ plasmas by ionizing neutral ^9Be atoms in a separate trap (not shown) and then transferring the ions to the main trap for experimentation.²⁰ This procedure can be

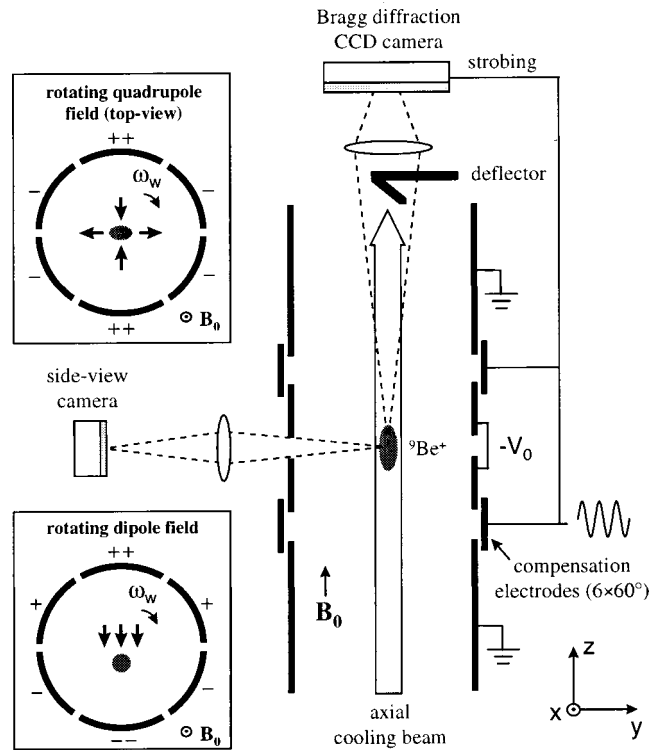


FIG. 1. Schematic side-view of the cylindrical trap with real-space imaging optics and Bragg diffraction detection system. Cross sections of the rotating dipole and quadrupole field (in the x - y plane) are shown separately in the two insets.

repeated several times to accumulate up to 10^6 ions. We expect that essentially all the ions in the trap are singly charged since the formation of doubly charged ions is energetically forbidden. While the total charge in the trap is conserved after loading, the relative abundance of contaminant ions increases from $<5\%$ for a new cloud on a time scale of 20 h, presumably due to reactions between $^9\text{Be}^+$ ions and background neutral molecules. By exciting ion cyclotron resonances, we determine that the two main contaminant ion species have mass 10 u and 26 u, where u is the atomic mass unit. These two species are likely to be BeH^+ and BeOH^+ , respectively. Unless noted, data presented in this paper are obtained on relatively clean clouds with $<10\%$ contaminant ions.

The trapped $^9\text{Be}^+$ ions are Doppler-cooled by two laser beams tuned slightly below the $2s^2S_{1/2}(M_I = 3/2, M_J = 1/2) \rightarrow 2p^2P_{3/2}(3/2, 3/2)$ resonant transition frequency (wavelength $\lambda \approx 313.11$ nm).¹⁹ These laser beams also optically pump most of the ions into the $2s^2S_{1/2}(3/2, 1/2)$ state. From previous experiments,^{19,20} we estimate that temperatures $T \lesssim 10$ mK can be obtained. Here $k_B T$ refers to the average ion thermal energy in a frame rotating with the plasma, which is typically much smaller than the average kinetic energy in the global rotation ($\sim 10^2$ K). The axial cooling beam (waist diameter ≈ 0.5 mm, power ≈ 50 μW), directed parallel to B_0 as shown in Fig. 1, cools the ion thermal motion while not affecting the global rotation. A second laser beam (not shown in Fig. 1) with a much smaller waist diameter (≈ 0.07 mm) is directed perpendicular to B_0 and is used

to compress the plasma and vary the rotation frequency. This beam is turned off during the Bragg scattering measurements.

When the cloud reaches thermal equilibrium at these cryogenic temperatures, the plasma Debye length becomes much smaller than its diameter $2r_0$ and axial length $2z_0$. The influence of image charges is negligible here due to the small dimensions of the plasma compared to the trap radius ($<10\%$). Consequently, the plasma forms a uniform density spheroid, bounded by $z^2/z_0^2 + (x^2 + y^2)/r_0^2 = 1$, with a rigid-body rotation frequency ω_r in the range $\omega_m < \omega_r < (\Omega - \omega_m)$.²⁰ The particle density n_0 is determined from ω_r according to $\omega_p^2 \equiv e^2 n_0 / \epsilon_0 m = 2\omega_r(\Omega - \omega_r)$, where ω_p is the plasma frequency.²⁰ The maximum density (Brillouin limit) $n_B \equiv \epsilon_0 B_0^2 / 2m = 5.9 \times 10^9 \text{ cm}^{-3}$ occurs at $\omega_r = \Omega/2$, the condition for Brillouin flow. In the frame rotating with the plasma, (x_r, y_r, z) , the $e\mathbf{v} \times \mathbf{B}$ Lorentz force gives rise to a radially confining pseudo-potential, and the effective vacuum trapping potential becomes

$$\Phi_r = \frac{m\omega_z^2}{2e} [z^2 + \beta(x_r^2 + y_r^2)], \quad (1)$$

where β is the radial trapping strength defined as

$$\beta \equiv \frac{1}{2} \left(\frac{\omega_p^2}{\omega_z^2} - 1 \right) = \frac{\omega_r(\Omega - \omega_r)}{\omega_z^2} - \frac{1}{2} > 0. \quad (2)$$

The parameter β determines the aspect ratio $\alpha \equiv z_0/r_0$ of the spheroid.^{20,29} We use an f/5 imaging system to detect resonantly scattered photons from the cooling beams and produce a side-view image of the ${}^9\text{Be}^+$ ions. From this side-view image, we measure α and obtain ω_r and n_0 .

For the typical conditions of $T \leq 10 \text{ mK}$ and $n_0 \geq 4 \times 10^8 \text{ cm}^{-3}$, we obtain a Coulomb coupling parameter

$$\Gamma \equiv \left(\frac{e^2}{4\pi\epsilon_0 a_{\text{WS}}} \right) \frac{1}{k_B T} > 200, \quad (3)$$

where the Wigner-Seitz radius a_{WS} is defined by $4\pi a_{\text{WS}}^3/3 \equiv n_0^{-1}$. This strong ion-ion coupling results in the formation of crystalline lattices, which are body-centered cubic (bcc) in nearly spherical plasmas ($\alpha \approx 1$) with ion number $N \geq 2 \times 10^5$.^{4,5} As shown in Fig. 1, Bragg-scattered light from the axial cooling beam is detected with a charge-coupled device (CCD) camera near the forward-scattering direction since the wavelength is much smaller than the lattice spacing ($\lambda \ll a_{\text{WS}}$).⁴ After passing through the trap, the axial cooling beam is deflected away from the lenses collecting the Bragg-scattered light.

III. RESULTS AND ANALYSES

A. General results for both rotating fields

When the rotating fields are first applied, their rotation frequency ω_w is set close to ω_r so that they interact strongly with the plasma. By measuring the photon scattering rate from the cooling beams for a fixed laser frequency, which is a function of the ion temperature, we have established that the ion temperature does not change significantly with the application of the rotating fields. Since the rotating fields

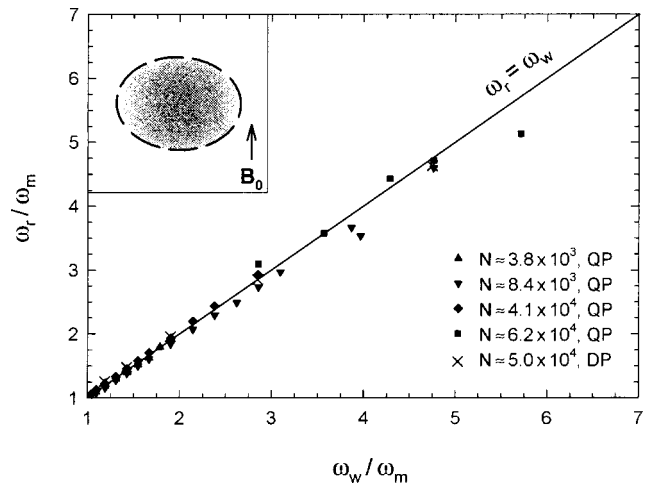


FIG. 2. The plasma rotation frequency ω_r versus the rotation frequency ω_w of the rotating fields. The frequency ω_r is determined from the aspect ratio α of several plasmas with $200 \leq V_0 \leq 1000 \text{ V}$. Solid symbols are with the quadrupole field and \times 's are with the dipole field. The inset shows a typical side-view image and its boundary fit to an ellipse (dashed line), giving α and ω_r .

typically cause less than 1% shape distortion to the plasma (see later discussions), the plasma rotation frequency ω_r can still be inferred from the aspect ratio α within the 5% uncertainty of this method. Furthermore, because Φ_r depends weakly on the ion mass for $\omega_r \ll \Omega/2$ as shown in Eq. (2), a multispecies plasma essentially has the same charge distribution as a pure ${}^9\text{Be}^+$ plasma except for the effect of centrifugal separation, in which the heavier ions tend to occupy positions at larger radii.³⁰ With a sufficiently large rotating field amplitude V_w , we are able to vary the plasma aspect ratio (and hence ω_r) by slowly changing ω_w . Figure 2 shows ω_r as determined from the side-view images versus ω_w with both the rotating dipole and quadrupole fields and for several plasmas with particle number $N < 7 \times 10^4$ and $\omega_r \ll \Omega/2$. The plasma rotation frequency ω_r tracks ω_w closely within the experimental accuracy, demonstrating external control of the plasma rotation by the rotating fields. The data of Fig. 2 were obtained at low temperatures ($T \leq 10 \text{ mK}$) with the axial cooling laser on continuously. However, we are also able to control the plasma rotation with the laser tuned far below the atomic transition frequency or blocked for short periods of time ($\sim 1 \text{ min}$). Under these conditions, we expect significantly higher plasma temperatures (up to $T \sim 10 \text{ K}$) so that the plasma is only weakly correlated ($\Gamma \sim 0.2$).

For a more accurate determination of ω_r , we use the time dependence of the laser light Bragg-scattered from the rotating crystals.^{4,5} A gateable image intensifier, installed in front of the CCD camera, allows the diffraction pattern to be recorded stroboscopically. Figure 3(a) shows a time-averaged diffraction pattern of concentric rings from an approximately spherical plasma with $N \approx 7.5 \times 10^5$. Even if this pattern is from a single crystal, rings are observed because of the plasma rotation about the axial laser beam.⁴ With the rotating field applied and controlling the plasma rotation, we trigger the intensifier synchronously with the rotating field opening the camera for 50 ns each $2\pi/\omega_w$ period. This en-

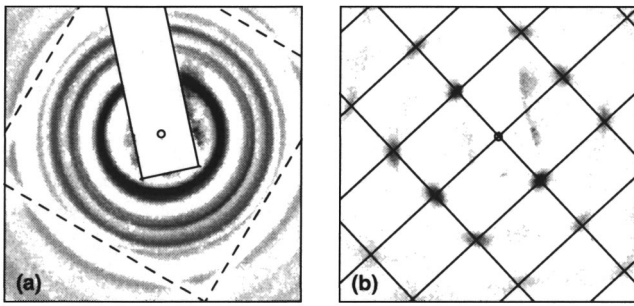


FIG. 3. Bragg diffraction patterns from a plasma phase locked to a rotating quadrupole field ($\omega_r = \omega_w = 2\pi \times 140$ kHz, $n_0 \approx 4.26 \times 10^8$ cm⁻³, $\alpha \approx 1.1$). (a) 1 s time-averaged pattern. The long rectangular shadow is from the deflector for the incident beam; four line shadows that form a square are due to a wire mesh at the exit window of the vacuum chamber. (b) Time-resolved pattern obtained by strobing the camera with the rotating field (integration time ≈ 5 s). A spot is predicted at each intersection of the rectangular grid lines for a bcc with a {110} plane perpendicular to the axial laser beam. The grid spacings are determined from n_0 and are not fitted.

ables the camera to record the diffraction pattern in the rest frame of the rotating field. Figure 3(b) shows such a time-resolved pattern taken nearly simultaneously with Fig. 3(a) and accumulated over $\sim 10^6$ plasma rotations. The well-defined rectangular dot pattern demonstrates that the crystal is phase locked to the rotating field. In this work, we could determine phase-locked rotation when \mathbf{B}_0 is aligned within 0.01° of the trap axis and for $\omega_r \lesssim \Omega/20$. This alignment is obtained by minimizing the amplitude of zero-frequency modes of the plasma.² Furthermore, the structure and spacings of the crystalline lattice and its orientation with respect to the laser beam can last longer than 30 min under this rotation control. For comparison, a particular Bragg scattering pattern typically changes after ~ 1 min without the rotating field control, perhaps due to effects from the plasma spin-down. With a weak rotating field amplitude or when the trap axis is tilted a few hundredth of a degree with respect to \mathbf{B}_0 , we cannot obtain phase locking but are able to stabilize the plasma rotation frequency close to the rotating field frequency with $\lesssim 1\%$ slippage.

B. Quadrupole field control

With the rotating quadrupole field, which has a potential $\propto (y^2 - x^2)\cos(2\omega_w t) + 2xy \sin(2\omega_w t)$, the equilibrium plasma surface is actually a spinning triaxial ellipsoid with three principal axes differing in length.²⁹ Since the plasma is phase locked with $\omega_r = \omega_w$, the combined vacuum trapping potential in the rotating frame becomes

$$\Phi'_r = \frac{m\omega_z^2}{2e} [z^2 + (\beta - \delta)x_r^2 + (\beta + \delta)y_r^2], \quad (4)$$

where $\delta = f_g V_w / V_0 \geq 0$ is the relative strength of the quadrupole field and f_g depends only on the trap geometry. Here electric fields from the ambient drag and image charges are neglected. The thermal equilibrium state in the frame rotating with the plasma is bounded by $z^2/z_0^2 + x_r^2/x_0^2 + y_r^2/y_0^2 = 1$ with $x_0 \geq y_0$. The parallel and perpendicular aspect ratios ($\alpha_{\parallel} \equiv z_0/y_0, \alpha_{\perp} \equiv x_0/y_0$) are determined by parameters β and δ .²⁹ This shape produces a space-charge potential which

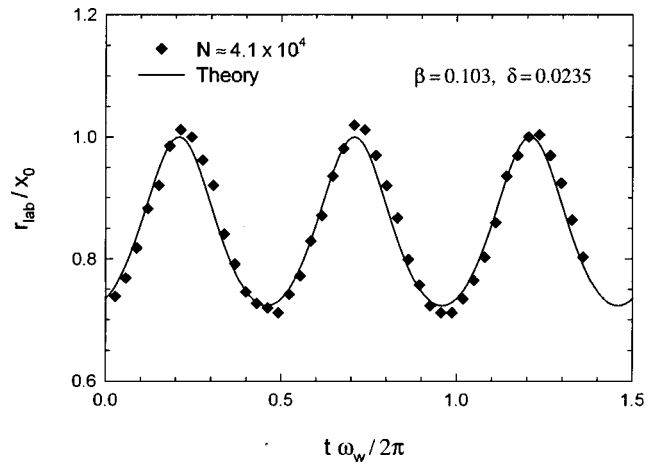


FIG. 4. Oscillation of the plasma radius r_{lab} of the side-view image with the rotating quadrupole field. The theory curve is calculated using the calibrated f_g from Fig. 5(a). The relative phase between the theory and data is not adjusted.

cancels Φ'_r within the equilibrated plasma. In this equilibrium, each individual ion still undergoes a purely rotational average motion as in the ordinary thermal equilibrium state without the rotating field.

To obtain an α_{\perp} significantly above one, we maximize the ratio δ/β by reducing V_0 to less than 200 V and setting ω_w close to the magnetron frequency ω_m . At these low rotation frequencies and with only the perpendicular cooling beam, the contaminant ions are well mixed with the $^9\text{Be}^+$ ions, making the boundary of the fluorescing $^9\text{Be}^+$ ions coincide with that of the plasma. Side-view images of the plasma are then recorded stroboscopically at different phases of the rotating field. The radius r_{lab} of the side-view image is expected to oscillate at $2\omega_w$, with an amplitude proportional to $x_0 - y_0$. Figure 4 shows a measurement of r_{lab} on a plasma with $\alpha_{\parallel} \approx 0.15$ and $\alpha_{\perp} \approx 1.4$, rotating at 2.5 kHz ($V_0 = 50$ V, $V_w \approx 185$ V). Excellent agreement between the theory and data is exhibited, showing that the plasma is indeed equilibrated with the rotating quadrupole field.

We have measured the dependence of α_{\perp} on parameters δ and β . Figure 5(a) shows α_{\perp} versus δ at fixed $\beta = 0.103$. Good agreement with the theory is obtained by fitting these data for f_g with the result $f_g \approx 6.38 \times 10^{-3}$. Figure 5(b) shows α_{\perp} versus β for fixed $\delta \approx 0.0159$ using the calibrated f_g value. Excellent agreement is again observed, showing the rapid decrease to unity for α_{\perp} as β is increased. Under typical conditions ($V_0 \geq 500$ V, $V_w \leq 50$ V, and $\omega_w \geq 1.1 \omega_m$, giving $\delta < 7 \times 10^{-4}$ and $\beta > 0.1$), $\alpha_{\perp} - 1$ is less than 1%. This small distortion, however, generates sufficient torque to phase lock the plasma rotation when the trap is nearly aligned with the magnetic field.

C. Dipole field control

We have examined rotation control using the dipole field with a potential $\propto y \sin(\omega_w t) - x \cos(\omega_w t)$. Theoretically, this field is not expected to provide rotation control for a single-species plasma in a quadratic trap. Instead, it drives only a “center-of-mass” orbital motion about the trap axis without

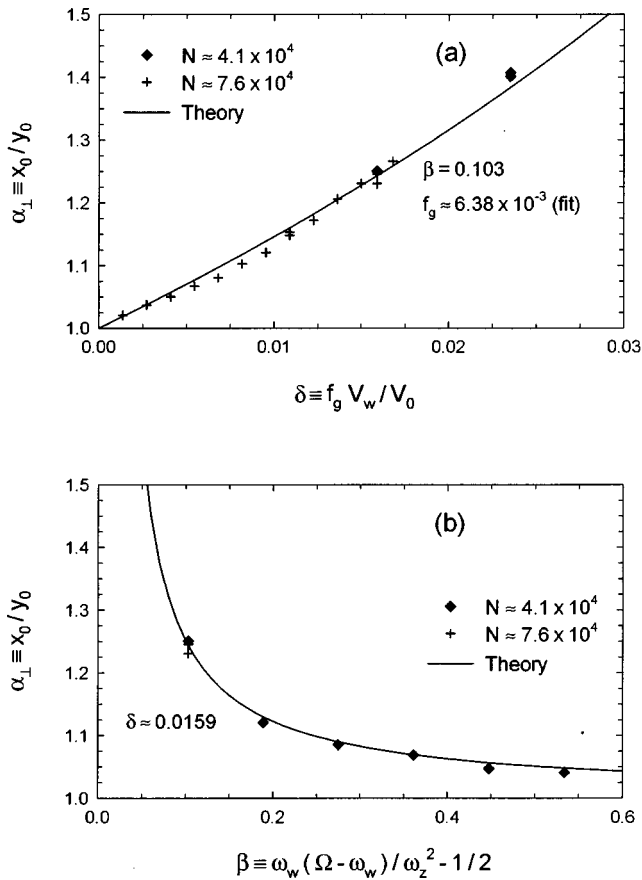


FIG. 5. Dependence of perpendicular aspect ratio α_{\perp} versus (a) rotating field strength δ and (b) radial trapping strength β . Two plasmas are used with $50 \leq V_0 \leq 100$ V and $15 \leq V_w \leq 185$ V. The geometric factor f_g is calibrated in (a).

surface distortions and is decoupled from the internal plasma rotation. Experimentally, however, rotation control including phase locking similar to that from the quadrupole field is obtained with the rotating dipole field as discussed in the previous sections. While the asymmetric field from image charges induced by the center-of-mass motion could provide the observed coupling to the plasma rotation, this field is too weak to be effective for our typical trap parameters.

Experimental evidence suggests that the coupling between the center-of-mass motion and plasma rotation is provided by the contaminant ions. By measuring the plasma dynamic response under sudden changes of the dipole field frequency²² we have observed that the torque from the dipole field increases with time, presumably due to the growing percentage of the contaminant ions. Figure 6 shows the evolution of plasma rotation frequency as $\omega_w/2\pi$ is suddenly changed by ± 5 kHz from 60 kHz (magnetron frequency $\omega_m = 2\pi \times 42.2$ kHz) at $\Delta t = 0$. The initial and final rotation frequencies of the plasma are equal to that of the dipole field as determined from time-resolved Bragg scattering measurements. The intermediate data points are derived from the aspect ratio of the side-view images assuming that the plasma goes through successive thermal equilibrium states during the evolution. The torque from the rotating dipole field has clearly increased from the 1-h-old plasma with ap-

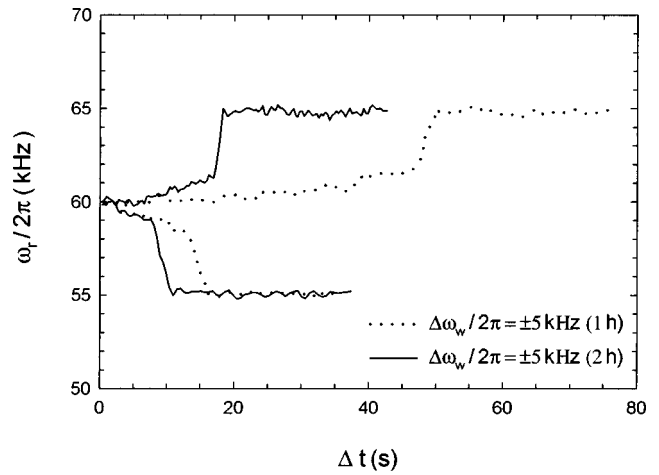


FIG. 6. Time evolution of the plasma rotation frequency under sudden changes of the dipole field frequency. Measurements on the same plasma 1 and 2 h after loading are plotted.

proximately 5% contaminant ions to the 2-h-old plasma with twice as many contaminant ions.

The effect of the contaminant ions on the plasma can be understood in terms of their azimuthally asymmetric distribution with the rotating dipole field. For typical rotation frequencies and laser cooling conditions, these heavier contaminant ions separate radially from the ${}^9\text{Be}^+$ ions and form a nonfluorescent outer cylindrical layer without the rotating field.^{30,31} As the plasma undergoes a driven center-of-mass circular motion with the rotating dipole field, the heavier contaminant ions distribute preferentially farther from the trap center than the ${}^9\text{Be}^+$ ions. In order for the contaminant ions to be distributed away from the trap center and to have rigid-body rotation, the plasma rotation frequency must match the rotation frequency of the dipole field (see discussions below). This produces a coupling between the driven center-of-mass motion and the plasma rotation, enabling the rotating dipole field control. When the plasma reaches ther-

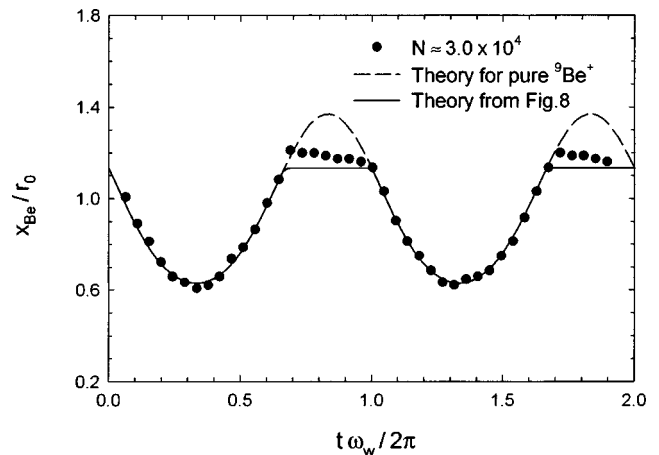


FIG. 7. Oscillation of the positive radial boundary x_{Be} with the rotating dipole field. The dashed curve is calculated for a pure ${}^9\text{Be}^+$ plasma and the solid curve is obtained from the simulation shown in Fig. 8. The dipole field amplitude at the plasma is derived by fitting the data, while the relative phase between the theories and data is not adjusted.

mal equilibrium with the rotating dipole field at $\omega_r = \omega_w$, the average ion motion is simply a rigid-body rotation about the trap axis at ω_w .

Figure 7 shows the position x_{Be} of the positive radial boundary (at $z=0$) from the side-view images of a plasma containing about 12% contaminant ions and phased locked with a dipole field rotating at 9 kHz (magnetron frequency is $2\pi \times 8.4$ kHz). This measurement is obtained with the same stroboscopic technique that was used for the quadrupole field results. For these conditions, however, the contaminant ions are well separated from the ${}^9\text{Be}^+$ ions due to the higher rotation frequency. For a pure ${}^9\text{Be}^+$ plasma, a periodic oscillation of x_{Be} at ω_w is expected due to the center-of-mass motion, as shown in Fig. 7. The data generally follow this prediction except for the ‘clipping’ of x_{Be} at certain phases of the rotating dipole field.

A Monte Carlo simulation on the equilibrium distribution of a two-species plasma (in the rest frame of the dipole field) is shown in Fig. 8. The plasma is made of 1000 particles with 88% ${}^9\text{Be}^+$ (dots) and 12% contaminant ions having mass 26 u (open circles), and is driven by a rotating dipole field resulting in the same relative displacement as in Fig. 7. The plasma has a very oblate shape which enhances its center-of-mass displacement as shown in the side-view of Fig. 8(b). In the x - y distribution shown in Fig. 8(a), the overall charge is distributed nearly symmetrically with respect to the shifted plasma axis, while the ${}^9\text{Be}^+$ ions and the contaminant ions are positioned asymmetrically inside the plasma. The boundary of the ${}^9\text{Be}^+$ ions is approximately made of two arcs: one, bordering the vacuum, is centered on the plasma axis (the \oplus symbol), and the other, bordering the contaminant ions, is centered on the trap axis (the cross). This shape explains the observed clipping of x_{Be} in Fig. 7. The small discrepancy between the data and the solid curve in Fig. 7 is likely due to an overestimation of the percentage of the contaminant ions from the side-view images without the rotating field.

When contaminant ions are present, it is advantageous to use the dipole rather than quadrupole field to control the plasma rotation because greater electric field strength at the plasma surface can be obtained for the same amplitude V_w on the compensation electrodes. This is because the plasma dimensions are typically much smaller than the trap radius and the dipole field decays much more gradually from the compensation electrodes than the quadrupole field. Rotation control in the range $\omega_m < \omega_r < (\Omega - \omega_m)$, which includes rotational equilibrium near Brillouin flow ($\omega_r = \Omega/2$), has been achieved using the rotating dipole field. For $\omega_r \sim \Omega/2$, crystalline lattices are generally not observed, and the aspect ratio α depends only weakly on the rotation frequency. However, we can infer ω_r by measuring the angle of the first Bragg scattering ring, θ_{scatt} , from ions in the shell structures. This angle is related to the Wigner–Seitz radius a_{WS} through

$$\theta_{\text{scatt}} a_{\text{WS}} \approx 4.4 \left(\frac{\lambda}{2\pi} \right), \tag{5}$$

where θ_{scatt} is in radian (see Ref. 4). The Wigner–Seitz radius in turn is determined by the plasma rotation frequency.

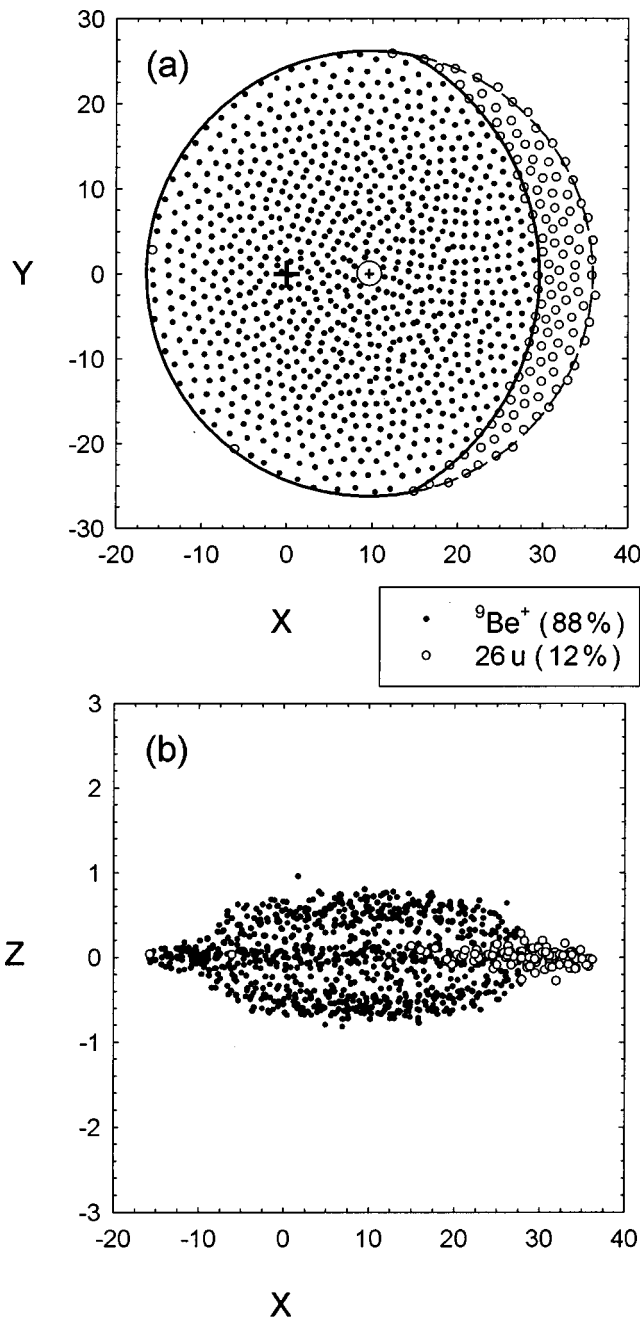


FIG. 8. A Monte Carlo simulation of the thermal equilibrium distribution of a two-species plasma with the rotating dipole field. The plasma is made of 1000 particles with 88% ${}^9\text{Be}^+$ and 12% contaminant ions having mass 26 u, and has a coupling parameter $\Gamma = 40$. The trapping parameters are the same as in Fig. 7. (a) The x - y distribution. Solid and dashed lines denote boundaries of the ${}^9\text{Be}^+$ ions and the plasma, respectively. (b) The x - z distribution with ten times smaller z scale.

Figure 9 shows the scattering angle θ_{scatt} as a function of the rotation frequency of the dipole field for two plasmas with different compositions of contaminant ions. With only heavier contaminant ions (dots), we can control the plasma rotation frequency up to about 0.9Ω (dotted vertical line) corresponding to the frequency at which ions having mass 10 u can no longer remain in the plasma. If we intentionally create some lighter ions (\times 's), we are able to control ω_r ,

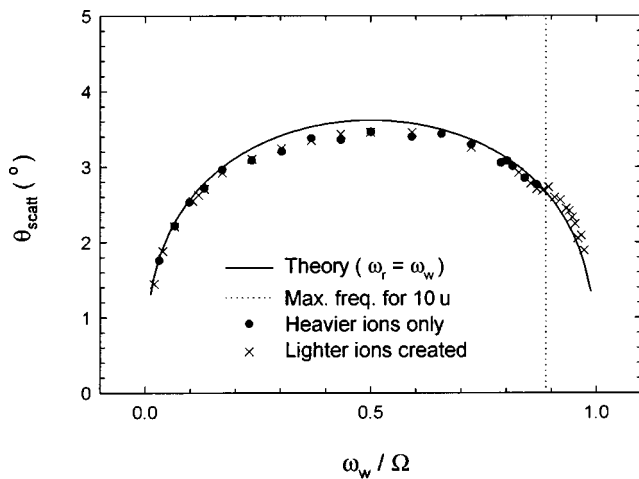


FIG. 9. The angle of the first Bragg scattering ring from shells versus the rotation frequency of the dipole field. Data from a plasma with only heavier contaminant ions are shown as dots. \times 's are data from a plasma with some lighter ions than ${}^9\text{Be}^+$.

through all allowed rotation frequencies. This observation provides further evidence that the contaminant ions are the main coupling mechanism for the rotating dipole field. We cannot, however, exclude the possibility that different non-ideal effects can cause sufficient coupling in other experiments.

IV. CONCLUSIONS AND DISCUSSION

We have shown experimentally that azimuthally asymmetric electric fields rotating in the same sense as the plasma can exert a torque that balances the ambient drag in both weakly and strongly coupled regimes, resulting in infinite confinement times. The torque from the rotating wall fields acts to bring the plasma to the same rotation frequency as the applied field. For strongly coupled plasmas with laser cooling, we obtain phase-locked rotation with the rotating field even though there is a finite ambient drag on the plasma. This phase-locked rotation is possible presumably because crystallized plasmas are capable of sustaining some stress without structure breakup. As a result of this observation, we are now able to precisely control plasma properties such as density and boundary shape.

There are other methods to inject angular momentum into the plasma and vary the rotation frequency. For example, by exciting an azimuthally asymmetric mode that travels in the same direction but faster than the plasma rotation, ω_r can be increased very effectively due to the global coherent resonance.^{16,32} The challenge of this approach is to remain on resonance with the mode as the plasma rotation frequency is increased. It may also be difficult to balance the heating from the mode excitation. In addition, this method will probably not result in rotation control as precise as the rotating field technique.

Substantial questions remain concerning the theoretical models which give quantitative predictions for the torque from the rotating fields.^{33,34} In the strongly coupled regime, such models that describe the experiment are lacking. For

uncorrelated plasmas at higher temperatures, two-dimensional rotating fields may not be able to generate enough torque to balance the ambient drag, and electric fields with nonzero z components may be required.²² Rotating field control of pure electron plasmas also needs further refinement to improve its capability.²³

In the future, direct imaging of individual ions in a crystallized plasma may be possible because of the phase-locked rotation. In addition, the increased crystal stability improves the prospect of observing the solid-liquid phase transition of strongly coupled plasmas. Dynamics of the Brillouin flow is also an interesting area for investigation. Finally, it may be possible to influence the formation of crystalline lattices with the rotating fields and other perturbations, enabling external control of the crystal orientation.

ACKNOWLEDGMENTS

We thank D. Wineland, T. O'Neil, and C. F. Driscoll for discussions, and B. Jelenković, R. Rafac, M. Young, M. Lombardi, and D. Sullivan for useful comments on the manuscript.

This work is supported by the Office of Naval Research.

¹J. H. Malmberg, C. F. Driscoll, B. Beck, D. L. Eggleston, J. Fajans, K. Fine, X.-P. Huang, and A. W. Hyatt, in *Non-neutral Plasma Physics*, edited by C. W. Roberson and C. F. Driscoll (American Institute of Physics, New York, 1988), p. 28.

²J. J. Bollinger, D. J. Wineland, and D. H. E. Dubin, *Phys. Plasmas* **1**, 1403 (1994).

³For recent results, see *Non-neutral Plasma Physics II*, edited by J. Fajans and D. H. E. Dubin (American Institute of Physics, New York, 1995).

⁴J. N. Tan, J. J. Bollinger, B. Jelenkovic, and D. J. Wineland, *Phys. Rev. Lett.* **75**, 4198 (1995); J. N. Tan, J. J. Bollinger, B. Jelenkovic, W. M. Itano, and D. J. Wineland, in *Physics of Strongly Coupled Plasmas*, edited by W. D. Kraeft and M. Schlanges (World Scientific, Singapore, 1996), p. 387.

⁵W. M. Itano, J. J. Bollinger, J. N. Tan, B. Jelenkovic, X.-P. Huang, and D. J. Wineland, *Science* **279**, 686 (1998).

⁶R. Blatt, P. Gill, and R. C. Thompson, *J. Mod. Opt.* **39**, 193 (1992); R. C. Thompson, *Adv. At. Mol. Phys.* **31**, 63 (1993).

⁷J. N. Tan, J. J. Bollinger, and D. J. Wineland, *IEEE Trans Instrum. Meas.* **44**, 144 (1995).

⁸G. Gabrielse, X. Fei, L. A. Orozco, R. L. Tjoelker, J. Hass, H. Kalinowsky, T. A. Trainer, and W. Kells, *Phys. Rev. Lett.* **65**, 1317 (1990).

⁹R. G. Greaves and C. M. Surko, *Phys. Plasmas* **4**, 1528 (1997).

¹⁰D. Schneider, D. A. Church, G. Weinberg, A. J. Steiger, B. Beck, J. McDonald, E. Magee, and D. Knapp, *Rev. Sci. Instrum.* **65**, 3472 (1994).

¹¹T. M. O'Neil, *Phys. Fluids* **23**, 2216 (1980).

¹²J. S. DeGrassie and J. H. Malmberg, *Phys. Fluids* **23**, 63 (1980).

¹³D. A. Moore, R. C. Davidson, S. M. Kaye, and S. F. Paul, in *Non-neutral Plasma Physics II* (Ref. 3), p. 118.

¹⁴Torques from rotating neutral gas are considered in A. J. Peurrung and S. E. Barlow, *Phys. Plasmas* **3**, 2859 (1996).

¹⁵J. H. Malmberg and C. F. Driscoll, *Phys. Rev. Lett.* **44**, 654 (1980); C. F. Driscoll, K. S. Fine, and J. H. Malmberg, *Phys. Fluids* **29**, 2015 (1986).

¹⁶D. L. Eggleston, T. M. O'Neil, and J. H. Malmberg, *Phys. Rev. Lett.* **53**, 982 (1984).

¹⁷J. Notte and J. Fajans, *Phys. Plasmas* **1**, 1123 (1994).

¹⁸D. L. Eggleston, *Phys. Plasmas* **4**, 1196 (1997).

¹⁹J. J. Bollinger and D. J. Wineland, *Phys. Rev. Lett.* **53**, 348 (1984).

²⁰L. R. Brewer, J. D. Prestage, J. J. Bollinger, W. M. Itano, D. J. Larson, and D. J. Wineland, *Phys. Rev. A* **38**, 859 (1988); D. J. Heinzen, J. J. Bollinger, F. L. Moore, W. M. Itano, and D. J. Wineland, *Phys. Rev. Lett.* **66**, 2080 (1991).

²¹Some preliminary results on Mg^+ plasmas are in F. Anderegg, X.-P. Huang, C. F. Driscoll, G. D. Severn, and E. Sarid, in *Non-neutral Plasma Physics II* (Ref. 3), p. 1.

- ²²X.-P. Huang, F. Anderegg, E. M. Hollmann, C. F. Driscoll, and T. M. O'Neil, *Phys. Rev. Lett.* **78**, 875 (1997).
- ²³A preliminary work on pure electron plasmas is in R. E. Pollock and F. Anderegg, in *Non-neutral Plasma Physics II* (Ref. 3), p. 139.
- ²⁴X.-P. Huang, J. J. Bollinger, T. B. Mitchell, and W. M. Itano, *Phys. Rev. Lett.* **80**, 73 (1998).
- ²⁵D. J. Wineland and H. G. Dehmelt, *Int. J. Mass Spectrom. Ion Processes* **16**, 338 (1974); **19**, 251(E) (1976).
- ²⁶L. S. Brown and G. Gabrielse, *Rev. Mod. Phys.* **58**, 233 (1986).
- ²⁷G. Savard, St. Becker, G. Bollen, H.-J. Kluge, R. B. Moore, Th. Otto, L. Schweikhard, H. Stolzenberg, and U. Wiess, *Phys. Lett. A* **158**, 247 (1991); S. Guan, X. Xiang, and A. G. Marshall, *Int. J. Mass Spectrom. Ion Processes* **124**, 53 (1993).
- ²⁸C. S. Weimer, J. J. Bollinger, F. L. Moore, and D. J. Wineland, *Phys. Rev. A* **49**, 3842 (1994).
- ²⁹D. H. E. Dubin and T. M. O'Neil, "Trapped non-neutral plasmas, liquids, and crystals (the thermal equilibrium states)," submitted to *Rev. Mod. Phys.*
- ³⁰T. M. O'Neil, *Phys. Fluids* **24**, 1447 (1981).
- ³¹D. J. Larson, J. C. Bergquist, J. J. Bollinger, W. M. Itano, and D. J. Wineland, *Phys. Rev. Lett.* **57**, 70 (1986).
- ³²T. B. Mitchell, Ph.D. thesis, University of California at San Diego, 1993, p. 58.
- ³³S. M. Crooks and T. M. O'Neil, *Phys. Plasmas* **2**, 355 (1995); S. M. Crooks, Ph.D. thesis, University of California at San Diego, 1995, p. 56.
- ³⁴R. Fitzpatrick and E. P. Yu, *Phys. Plasmas* **4**, 917 (1997).